Survey of Cirrus and atmospheric properties from TOVS Path-B: Natural variability and impact of air traffic on cirrus coverage

C. J. Stubenrauch and Atmospheric Analysis (ARA) Group[1], U. Schumann[2]

[1]C.N.R.S. / IPSL - Laboratoire de Météorologie Dynamique, Ecole Polytechnique, Palaiseau, France
[2]Deutsches Zentrum für Luft- und Raumfahrt, Institut für Physik der Atmosphäre, Oberpfaffenhofen, Germany

Abstract

The TOVS Path-B data set provides atmospheric temperature and water vapor profiles as well as cloud properties over the globe, from 1987 to 1995. Their relatively high spectral resolution yields reliable cirrus properties, day and night. First, we present average cirrus properties and their seasonal and diurnal variations. A reanalysis which will extend the present data set back to 1979 and up to now is at present in preparation.
Upper tropospheric relative humidity with respect to ice has been computed from specific humidity over an atmospheric layer between 300 and 100 hPa by using the retrieved temperature profiles. Upper tropospheric relative humidity distributions of clear sky are slightly narrower than those of thin cirrus, but few clear sky scenes are also ice saturated in agreement with other observations.
An example of an analysis combining information on upper tropospheric relative humidity and cirrus coverage is given in the investigation of the impact of air traffic on cirrus formation. Contrails form when the hot and humid exhaust gases from the combustion of fuels by an aircraft mix with the ambient, cold atmosphere. Their persistence depends on upper tropospheric relative humidity. Trends of seasonal mean effective high cloud amount have been analyzed in regions with high and low air traffic density. In regions with especially high air traffic density, a significantly stronger increase of effective high cloud amount is found for situations with sufficiently cold and humid air masses favorable for contrails than for all situations in general.

Data

The TOVS Path-B data set (Scott et al. 1999) provides atmospheric temperature and water vapor profiles as well as cloud and surface properties at a spatial resolution of 1° latitude x 1° longitude, from 1987 to 1995. Their relatively high spectral resolution yields reliable cirrus properties, day and night (Stubenrauch et al. 1999a). For large-scale semi-transparent cirrus (visible optical thickness between 0.7 and 3.8), bulk microphysical properties have been retrieved, using spectral cirrus emissivity differences between 11 and 8 μm (Rädel et al. 2003, Stubenrauch et al. 2004a).
The inversion algorithm (Chédin et al. 1985) which converts the measured radiances into physical properties of the atmosphere and surface is based on a fast line-by-line radiative transfer model (4A, Scott and Chédin 1981, http://www.ara.lmd.polytechnique.fr) and a climatological data set for the initial guess of the atmospheric temperature profile retrieval (Chevallier et al. 1998). This Thermodynamic Initial Guess Retrieval (TIGR) data set has been generated from a huge

collection of radiosonde measurements of temperature, humidity and pressure that are grouped by atmospheric conditions, relating clear sky HIRS radiances to these atmospheric profiles. Systematic biases due to the radiative transfer model, instrument calibration and unexpected events (such as the Mt Pinatubo eruption) are removed by applying corrections to the measured HIRS brightness temperatures. These bias adjustment corrections were obtained from a collocated radiosonde-satellite data set, provided by the National Satellite Data and Information Service (NESDIS) of NOAA for the period between 1987 and 1995.

To extend the TOVS Path-B data set, a similar collocated data set has been created from the complete radiosonde collection of the European Centre for Medium Range Weather Forecasts (ECMWF) and TOVS data. A complex quality control procedure followed by a clear sky identification algorithm has been developed, and the channel biases have been determined and are in the process of being evaluated.

After a multi-spectral cloud detection (Stubenrauch et al. 2004b), the HIRS radiances are averaged separately over clear pixels and over cloudy pixels within 100 km x 100 km regions. The average cloud-top pressure p_{cld} and the average effective cloud emissivity ε_{cld} over cloudy pixels are obtained from four radiances in the 15 μm CO_2-absorption band (with peak responses from 400 to 900 hPa levels in the atmosphere) and one in the 11 μm IR atmospheric window by minimizing a weighted χ^2 (Stubenrauch et al. 1999b). Empirical weights reflect the effect of the brightness temperature uncertainty within a TIGR air mass class on these radiances at the various cloud levels. Cloud height of the revised TOVS Path-B data set has been evaluated (Stubenrauch et al. 2005) by using vertical profiles of backscattered radiation from quasi-simultaneous Lidar In Space Technology Experiment (LITE). The cloud height determined by TOVS corresponds in general well to the height of the 'apparent middle' of the cloud system.

In the case of clear sky and thin clouds, the vertical distribution of specific humidity is obtained by using a neural network approach on channels most sensible to water vapour absorption combined with those sensitive to tropospheric temperature (Chaboureau et al. 1998). Due to the relatively coarse resolution of the channels sensitive to water vapour, the TOVS instruments only provide water vapor integrated over relatively large height intervals. Upper tropospheric relative humidity with respect to ice, U^{ice}, is therefore computed from the specific humidity integrated over atmospheric layers between 300 and 100 hPa (or between 500 and 300 hPa), W, and using the retrieved temperature in pressure steps of about 25 hPa, T(p):

$$U^{ice}(\Delta p) = \frac{g\rho W}{0.622 \int\limits_{100-300\,hPa} dp e_{sat}^{ice}(T(p)) / \left[p - (1-0.622) e_{sat}^{ice}(T(p))\right]}$$

with gravity g, density ρ and saturated partial water vapor pressure e_{sat}^{ice} with respect to ice (Sonntag 1990), which is determined from the temperature profile within the height interval.

High Cloud properties

Table 1 gives an overview of total and high cloud amount over the globe and selected regions, averaged from 1987 to 1995, as obtained from TOVS Path-B and ISCCP (Rossow and Schiffer

1999). ISCCP D2 data provide monthly averages and cloud type statistics over 2.5 ° latitude x 2.5° longitude, from 3-hourly observations of imagers aboard geostationary and polar satellite imagers. The TOVS Path-B averages shown in Table 1 are from NOAA-10/12 data, with local observation time at 7h30 am and 7h30 pm. High clouds are defined by p_{cld}<440 hPa, and are divided into three types, according to effective cloud amount $N\varepsilon_{cld}$ (> 0.95, 0.95-0.5 and < 0.5) by TOVS and visible optical thickness, τ_{cld}, (> 23, 3.6–23 and < 3.6) by ISCCP, as deep convection (cumulonimbus), cirrus and thin cirrus. About 70% of the Earth's surface is covered by clouds, with about 10% more cloudiness over ocean than over land. The cover of high clouds is about 30%, with a maximum of about 47% in the tropics. Due to their relatively high spectral resolution, IR vertical sounders are more sensitive to cirrus than imagers; therefore TOVS Path-B indicates 8% more cirrus over the globe and up to 20% more cirrus in the tropics than ISCCP.

Table 1. Eight-year average cloud type amounts from TOVS Path-B and ISCCP (italic), over the globe, NH midlatitudes (30°N-60°N), tropics (20°N-20°S) and SH midlatitudes (30°S-60°S).

Cloud type amounts (%)	global		ocean		land	
all	73	*67*	74	*71*	69	*58*
Deep convection	2.4	*2.8*	1.9	*2.8*	3.5	*2.7*
Cirrus + thin cirrus	27.3	*19.1*	26.9	*18.0*	27.8	*21.7*

Cloud type amounts (%)	NH midlatitudes		tropics		SH midlatitudes	
Deep convection	3.0	*3.3*	3.5	*2.5*	2.4	*3.0*
Cirrus + thin cirrus	27.7	*20.3*	44.8	*24.9*	21.8	*16.5*

Figures 1 present time-series of frequencies of occurrence (weighted by the fraction covering the 1° x 1° grids) of cumulonimbus, cirrus and thin cirrus as obtained from TOVS Path-B, for NH midlatitudes, tropics and SH midlatitudes. Data are averaged from NOAA10 and NOAA12 satellites from 1987 to 1995 for observation times 7:30 and 19:30 LUT. In the tropics there are slightly more thin cirrus (24%) than cirrus (21%). The midlatitudes are covered by about 15% cirrus, but the amount of thin cirrus is higher in the NH (10% compared to 7.5% in the SH). In the NH midlatitudes *thin cirrus* have a pronounced seasonal cycle whereas *cirrus* do not have a seasonal cycle. However, in the SH midlatitudes *cirrus* have a pronounced seasonal cycle and *thin cirrus* have no seasonal cycle. During the period of eight years, these high cloud amounts are quite stable.

The seasonal cycle of effective high cloud amount is stronger over land than over ocean. It is strongest in the subtropics due to the moving of the InterTropical Convergence Zone towards the summer hemisphere. Over tropical land the diurnal variability is stronger than the seasonal variability.

Figures 2 present the diurnal cycles of frequency of occurrence of the three high cloud types shown in Figures 1, separately in the tropics, subtropics and midlatitudes. In each figure the diurnal cycle is shown for land and for ocean, in January and in July. For subtropics and midlatitudes NH and SH values are shown in green and blue respectively. The drifting of the

NOAA11 satellite made it possible to use four observation times: 2:00 and 14:00 LUT from 1989 to 1990 and 4:30 and 16:30 LUT from 1993 to 1994. From these figures we conclude that

- in general diurnal cycles are strongest over land in the tropics and in summer,
- the maximum of convection occurrence is in the evening,
- maximum cirrus occurrence happens during night and decreases during the day,
- maximum of thin cirrus occurrence is in the early afternoon.

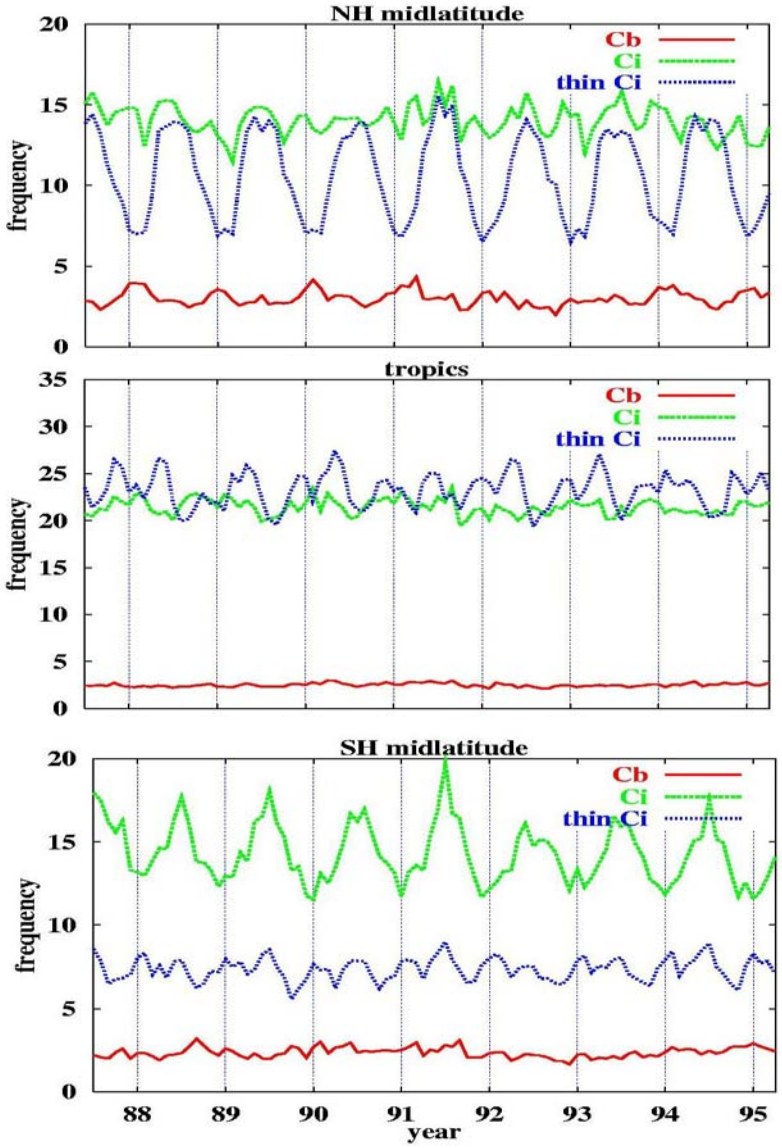

Fig. 1: Time series of frequency of occurrence of different high cloud types over the eight-year period of TOVS Path-B, separately in NH midlatitudes, tropics and SH midlatitudes.

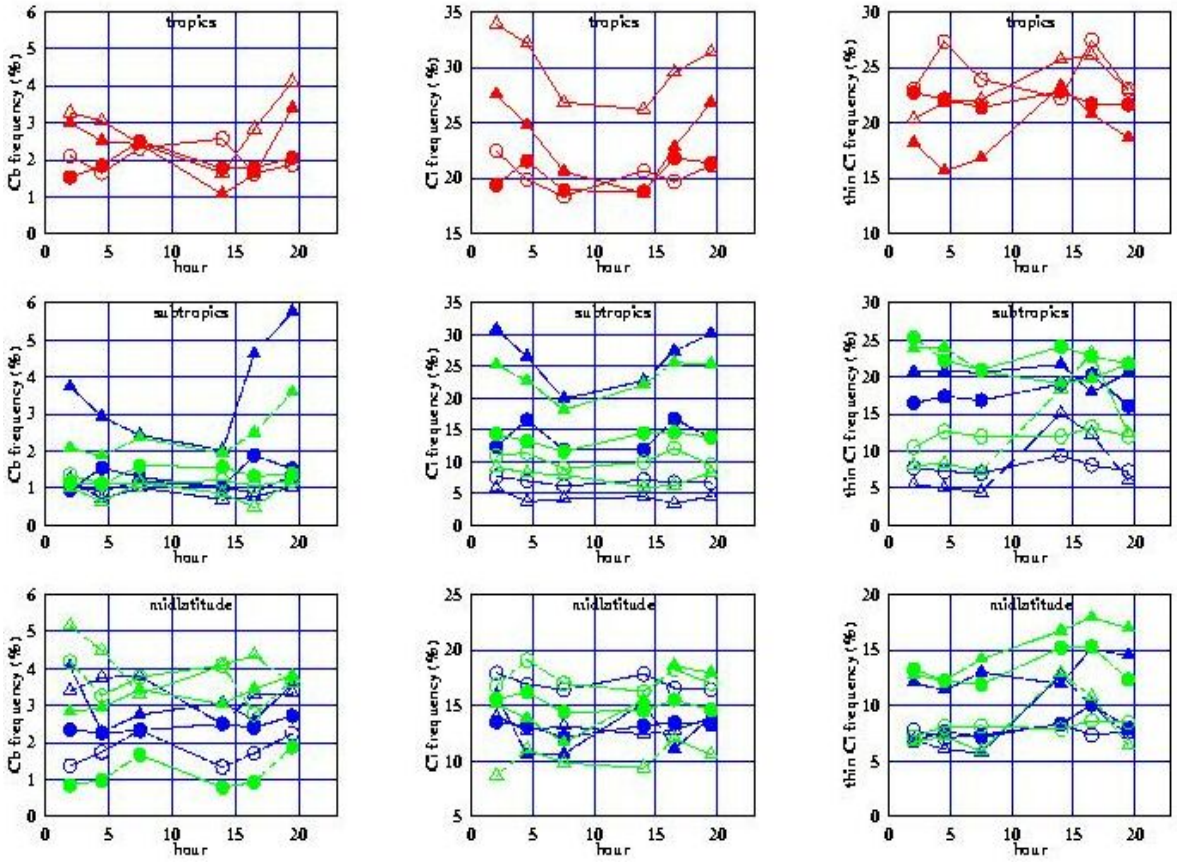

Fig. 2: Diurnal cycles of frequency of occurrence of different high cloud types, separately in tropics, subtropics and midlatitudes. For subtropics and midlatitudes NH and SH values are shown in green and blue, respectively. In each figure the diurnal cycle is shown for land (triangles) and for ocean (points), in January (open) and in July (filled).

Upper tropospheric humidity

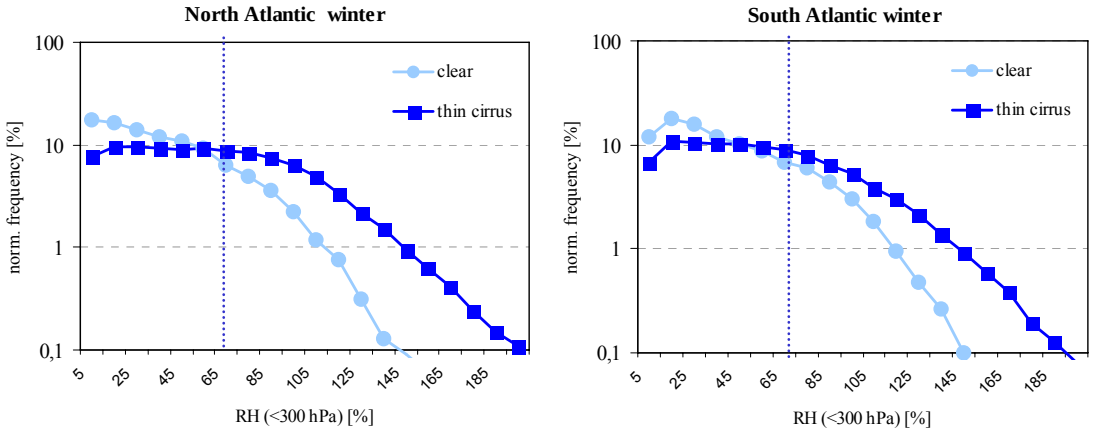

Fig. 3: Upper tropospheric relative humidity distributions for situations with clear sky and with thin cirrus: over the North Atlantic (30°N-60°N and 0°-60°W) in winter (left) and over the South Atlantic (30°S-60°S and 0°-60°W) in winter (right).

Figures 3 present frequency distributions (normalized to the same integral) of upper tropospheric relative humidity integrated over an atmospheric layer between 300 and 100 hPa, separately for situations with clear sky and with thin cirrus. North Atlantic and South Atlantic, both during the winter season, are compared. Clear sky distributions are slightly narrower than those of thin cirrus, but few clear sky scenes are also ice saturated, in agreement with other observations (Gierens et al. 1999). The shapes of the distributions of both regions are similar.

Impact of air traffic on cirrus

The increase in anthropogenic aerosols and in air traffic has led to theoretical and observational investigations of their impact on the formation of cirrus clouds. Contrails form when the hot and humid exhaust gases from the combustion of fuels by an aircraft mix with the ambient, cold atmosphere (Schumann 1996). Their persistence depends on upper tropospheric humidity and temperature (Sausen et al. 1998).

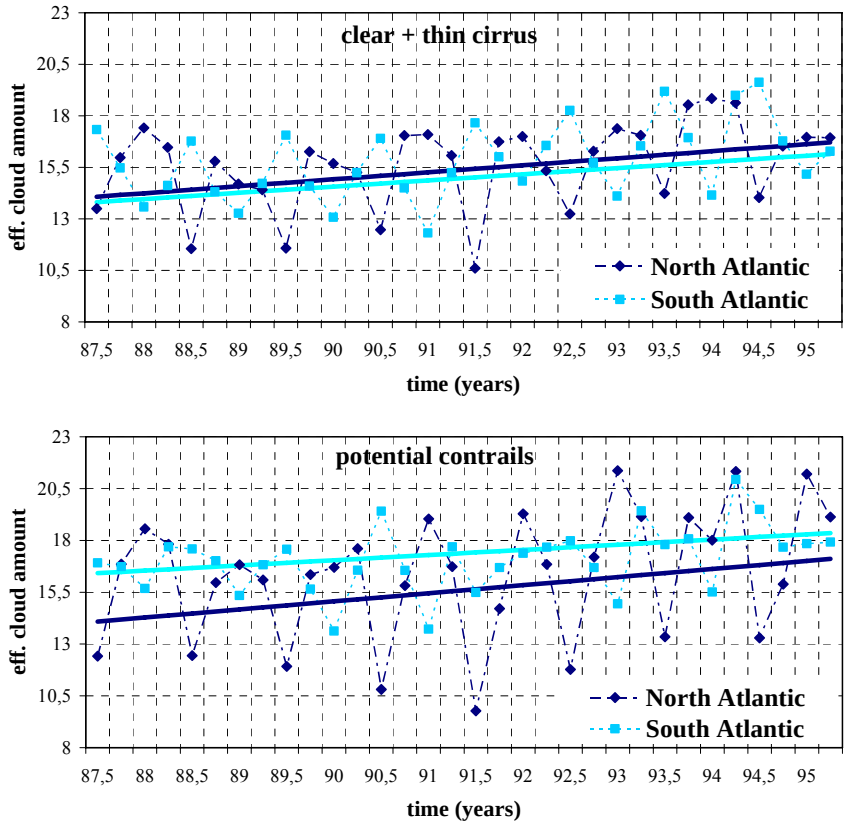

Fig. 4: Time series of seasonal effective high cloud amount over North Atlantic and over South Atlantic with linear fits taking into account statistical errors (which are small) a) for all situations (clear sky and thin cirrus) and b) for situations favorable to contrail formation.

Cirrus evolve when the upper tropospheric relative humidity with respect to ice exceeds the saturation humidity over ice, while contrails form already when the relative humidity is below

this value but exceeds a critical value, U*, depending on temperature and a parameter depending on the fuel used by the aircraft (Schumann 1996). For Kerosene and at a pressure of 230 hPa, the maximum temperature for contrail formation is about 233 K. Upper tropospheric relative humidity from TOVS is used to distinguish situations labeled:

1) with cirrus ($U^{ice}(\Delta p)>0.7$),

2) with possible contrail occurrence ($U^{ice}(\Delta p)<0.7$ and $U^{liq}(\Delta p)>0.4\ U^{*}(\Delta p)$) and

3) with clear sky ($U^{ice}(\Delta p)<0.7$ and $U^{liq}(\Delta p)<0.4\ U^{*}(\Delta p)$).

The scaling factors 0.7 and 0.4, which take into account that the height interval Δp is much larger than the geometrical thickness of cirrus and contrails, have been obtained iteratively by considering the occurrence frequency and the effective high cloud amount of these three scene types.

As shown in Figs. 3, the upper tropospheric relative humidity distributions of North Atlantic (NA) and South Atlantic (SA) look quite similar, and therefore we use these two regions to contrast cirrus behavior under high air traffic density (NA) and low air traffic density (SA).We compare in Figures 4 the time series of seasonal averages of effective amount of high clouds over the North Atlantic and over the South Atlantic for all situations (1,2 and 3) and only for situation 2. Linear fits taking into account statistical errors are also shown. Whereas the effective high cloud amount increases at about the same rate (0.34 % and 0.30 % per year, respectively) over the NA compared to the SA, a slightly stronger increase is observed over the NA than over the SA when isolating situations favorable to contrail formation: 0.39 % per year compared to 0.25 % per year, for the eight-year period.

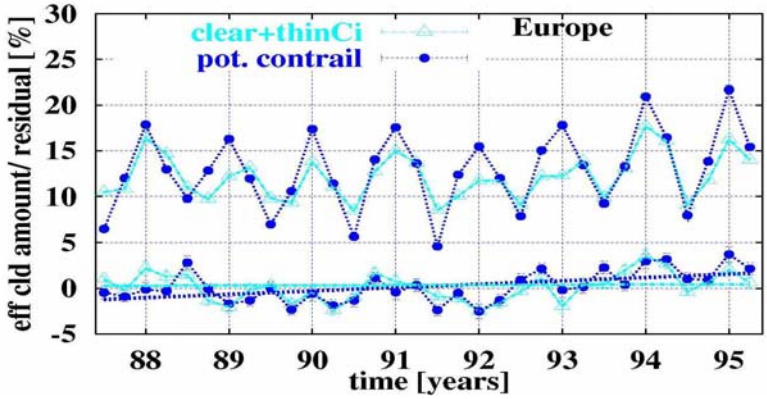

Fig. 5: Time series of seasonal effective high cloud amount (above) and residuals from eight-year seasonal averages (below) over Europe. Linear fits take into account statistical errors for all situations (clear sky and thin cirrus) and for situations favorable to contrail formation.

As an example of a region with very high air traffic density we consider Europe (40°N-60°N and 0°-40°E) for which Fig. 5 compares time series of seasonal effective high cloud amount as well as the residuals between these values and the eight-year seasonal averages for all situations and for situations with potential contrails. Linear tendencies show no trend for all situations and an increase of effective high cloud amount of about 0.37 % per year in situations favorable to contrail formation. Within the statistical errors, the confidence levels of the fits are larger than

99%. The difference in trends of effective high cloud amount between potential contrail situations and cirrus or between potential contrail situations and all situations could be used as an indicator of cirrus increase due to air traffic increase. Over Europe, this difference amounts to 2.8% or 3.5% per decade, respectively.

However, situations of potential contrails only occur in about 5 to 10 % of all situations. Weighted by frequency of potential contrail occurrence, the overall increase amounts to at least 0.20 % - 0.25 % per decade over regions with very high air traffic. A detailed analysis and results will be published in (Stubenrauch and Schumann 2005).

References

Chaboureau, J.-P., Chédin, A. and Scott, N.A. 1998. N. A. Remote sensing of the vertical distribution of atmospheric water vapor from the TOVS observations : Method and validation. *J. Geophys. Res.,* **103**, 8743-8752.

Chédin, A., Scott, N.A., Wahiche, C. and Moulinier, P. 1985. The improved initialization inversion method: A high resolution physical method for temperature retrievals from satellites of the TIROS-N series. *J. Climate Appl. Meteor*., **24**, 128-143.

Chevallier, F., Cheruy, F., Scott, N.A., and Chédin, A. 1998. A neural network approach for a fast and accurate computation of longwave radiative budget. *J. Appl. Meteor.,* **37**, 1385-1397.

Gierens, K., Schumann, U., Helten, M., Smit, H. and Marenco, A. 1999. A distribution law for relative humidity in the upper troposphere and lower stratosphere derived from three years of MOZAIC measurements. *Ann. Geophysicae,* **17**, 1218-1226.

Rädel, G., Stubenrauch, C.J., Holz, R. and Mitchell, D.L. 2003. Retrieval of Effective Ice Crystal Size in the Infrared : Sensitivity Study and Global Measurements from the TIROS-N Operational Vertical Sounder. *J. Geophys. Res.* **108**, 10.1029/ 2002JD002801.

Rossow, W.B. and Schiffer, R.A. 1999. Advances in understanding clouds from ISCCP. *Bull. Amer. Meter. Soc.,* **80**, 2261-2287.

Sausen, R., Gierens, K., Ponater, M. and Schumann, U. 1998. A diagnostic study of the global distribution of contrails. Part I: Present day climate. *Theor. Appl. Climatol*., **61**, 127-141.

Schumann, U. 1996. On conditions for contrail formation from aircraft exhausts. *Meteorol. Z.,* **5**, 2-23.

Scott, N.A., and Chédin, A. 1981. A fast line-by-line method for atmospheric absorption computations: the 4A Automized Atmospheric Absorption Atlas. *J. Appl. Meteor.,* **20**, 801-812.

Scott, N.A., Chédin, A., Armante, R., Francis, J., Stubenrauch, C.J., Chaboureau, J.-P., Chevallier, F., Claud, C. and Chéruy, F. 1999. Characteristics of the TOVS Pathfinder Path-B data set. *Bull. Amer. Meteor. Soc.,* **80**, 2679-2701.

Sonntag, D. 1990. Important new values of the physical constants of 1986, vapor pressure formulation based on the ITS-90 and psychrometer formulae. *Z. Meteorol.,* **70**, 340-344.

Stubenrauch, C.J., Rossow, W. B., Scott, N.A. and Chédin, A. 1999a. Clouds as seen by Infrared Sounders (3I) and Imagers (ISCCP): Part III) Spatial Heterogeneity and Radiative Effects. *J. Climate*, **12**, 3419-3442.

Stubenrauch, C.J., Chédin, A., Armante, R. and Scott, N.A. 1999b. Clouds as seen by Infrared Sounders (3I) and Imagers (ISCCP): Part II) A New Approach for Cloud Parameter Determination in the 3I Algorithms. *J. Climate*, **12**, 2214-2223.

Stubenrauch, C.J., Eddounia, F. and Rädel, G. 2004a. Correlations between microphysical properties of large-scale semi-transparent cirrus and the state of the atmosphere. *Atmos. Res.,* **72**, 403-423.

Stubenrauch, C.J., and the CIRAMOSA team 2004b. final report on the European Environmental project EVK2-CT-2000-00063, 99 pp., available at:
http://www.lmd.polytechnique.fr/CIRAMOSA/Welcome.html.

Stubenrauch, C.J., Eddounia, F. and Sauvage, L. 2005. Cloud heights from TOVS Path-B: Evaluation using LITE observations and distributions of highest cloud layers, *J. Geophys. Res.,* in press.

Stubenrauch, C.J. and Schumann, U. 2005. Impact of air traffic on cirrus coverage. *Geophys. Res. Lett.*, in press.

INTERNATIONAL ATOVS WORKING GROUP

Proceedings of the Fourteenth International TOVS Study Conference

Beijing, China
25-31 May 2005